POLITECNICO DI TORINO
Repository ISTITUZIONALE

Multifidelity Framework for the Efficient Identification of Damages in Complex Aerospace Systems

(Article begins on next page)

17 December 2025

Multifidelity Framework for the Efficient Identification of Damages in Complex Aerospace Systems

F. Di Fiore*, P. C. Berri [†] and L. Mainini [‡]
Politecnico di Torino, Torino, Italy, 10129

Next generation aircraft require the development and integration of a deal of innovative technologies to meet the ambitious sustainability goals set for aviation. This transformational effort is associated with a tremendous increase of the complexity of the onboard systems and their multiphysics coupled behaviours. A critical aspect relates to the characterization of the coupled fault modes resulting from the integration of these novel technologies, which introduce identifiability issues and demand new approaches for the efficient identification of (multimodal) non-nominal conditions. Model-based fault detection and identification (FDI) has been proven essential to infer onboard systems' health from signal acquisitions, but existing methods are too expensive and fail to capture incipient faults in presence of multimodality which prevent scaling to complex multiphysics systems. This work introduces a multifidelity framework to accelerate the identification of fault modes affecting complex systems. An original two-stage compression computes an optimally informative and highly reduced representation of the monitoring signals for the minimum demand of onboard resources. A multifidelity scheme for Bayesian inversion is developed to infer multidomain fault parameters from the compressed signals: variable cost and fidelity models are optimally queried for a major reduction of the overall computational expense. The framework is demonstrated and validated for aerospace electromechanical actuators affected by incipient multimodal faults. Remarkable accelerations of the FDI procedure are observed and the exact identification of the incipient fault condition achieved one order of magnitude faster than with standard algorithms.

I. Introduction

Modern aerospace systems require innovative multi-level and multiphysics technologies to meet the ever-increasing demand for performance and reliability during the operations in extreme environments. In addition, sustainability goals require the large introduction of novel technologies that further increase the level of complexity and physical couplings between subsystems [1, 2]. In this scenario, the identification of incipient multiphysics and multimodal faults constitutes a significant challenge: the growth of complexity hinders the adequate anticipation of this faults to support the safety-critical decision making procedures during flight operations [3].

Model-based Fault Detection and Identification (FDI) techniques permit to infer the fault condition of a system from measurements of signals sensitive to damages. The health assessment task is addressed solving an inverse problem: the actual damages affecting the system minimize the discrepancy between the diagnostic signal measured from the real system and the same signal simulated with a monitoring model [4–6]. Model-based FDI approaches have been successfully employed for the health assessment of aerospace systems. Examples include the work of Kolcio [7] where faults of the attitude control subsystem of a spacecraft are identified comparing real-world measurements with a fast simplified numerical model. Omata et al. [8] develop a model-based FDI framework for the health monitoring under uncertainties of reusable rocket engines, and adopt simplified system-level simulations as monitoring model to contain the overall cost of the procedure. Dalla Vedova et al. [9] address the FDI problem of an aerospace electromechanical actuator through a genetic algorithm, and use a simplified physics-based monitoring model to reduce the computational burden associated with the identification of mechanical and electrical faults. Kawatsu et al. [10] propose an FDI methodology for the health assessment of electromechanical actuators adopted for liquid rocket engines applications, where the monitoring signals are collected offline through multiphysics simulations.

Model-based FDI approaches show several limitations that affect the inference capabilities of multiphysics and multimodal incipient faults. Existing methodologies usually require a large amount of monitoring signal evaluations

---

*PhD. Student, Department of Mechanical and Aerospace Engineering, francesco.difiore@polito.it, AIAA Member.
[†]Affiliate, Department of Mechanical and Aerospace Engineering, piercarlo.berri@polito.it, AIAA Member.
[‡]Visiting/Adjunct Professor, Department of Mechanical and Aerospace Engineering, laura.mainini@polito.it, AIAA Associate Fellow.

through high-fidelity models of the system – e.g. numerical solution of partial differential equations or lumped parameter numerical models – that prohibitively increase the computational cost for the inference procedure. In practice, standard model-based techniques rely on low-fidelity monitoring models to relief the computational burden through either simplified physics assumptions or emulators built on dataset collected offline – e.g. via model reduction and surrogate modelling techniques. However, these approaches are not suitable for the robust inference of multiphysics incipient faults: the former simplified models might not be adequate to depict nonlinearities and multiphysics couplings, while the latter emulators might require massive high-fidelity evaluations to approximate the system dynamics. Further difficulties arise from the multimodal nature of these faults, which challenges identifiability and requires high-fidelity data to prevent erroneous health assessments. In addition, this scenario is complicated by the high-dimensionality of the diagnostic signals, which are measured with an high acquisition frequency to ensure representativeness of the system health status. These limitations preclude the scalability of model-based FDI methodologies for complex multiphysics systems, and hinder the reliable identification of complex faults affecting innovative components.

To address these limitations, this paper proposes an efficient computational framework for FDI that embeds high-fidelity models during the inference procedure, and accelerates the accurate identification of incipient faults affecting complex systems. In particular, our strategy is based on the original combination of i) a two-stage optimal compression of the diagnostic signal to reduce the dimensionality of the FDI procedure, and ii) a multifidelity Bayesian scheme for inversion to address the FDI problem and contain the high-fidelity calls. The two-stage compression strategy computes an optimal reduced representation of the diagnostic signal that retains only the most informative elements sensitive to faults. Two projection stages are used to compute this encoding map of the signal throught a combination of Dynamic Mode Decomposition (DMD) and Self Organizing Map (SOM). The inference of faults from the compressed signal is addressed through a multifidelity Bayesian scheme, which leverages and combines multiple models of the system at different levels of fidelity to effectively identify the health status of the system. The scheme is developed to embed high-fidelity simulations during the inference stage and aims at improving the effectiveness of the diagnostics; at the same time, lower-fidelity models are used to alleviate the computational cost of the procedure and more efficiently explore potential faults affecting the system.

We demonstrate and validate our FDI computational framework for the health assessment of an Electro-Mechanical Actuator (EMA) adopted in aircraft flight controls. EMA is an enabling technology toward sustainable aviation and more/all electric aircraft paradigms [11–13]. However, the fault detection and identification procedure of those systems represents a challenging task: the multidisciplinary nature of EMAs embeds multiphysics and coupled multimodal failure modes difficult to be detected in advance. This precludes their adoption for safety critical applications on board of the future generation of aircraft. We investigate the performance of our algorithm for both numerical and physical experiments on an EMA affected by mechanical and electrical incipient faults. It is shown that the proposed methodology provides substantial accelerations of the FDI procedure, and leads to the accurate identification of the EMA health status in numerical and physical tests.

The remaining of this paper is organized as follows. Section II describes the model-based FDI problem we aim to address in this work. Section III presents our multifidelity FDI approach in details and Section IV illustrates the demonstrative health monitoring problem of an aerospace EMA. In Section V, both the numerical and physical results achieved with our method are discussed. Finally, concluding remarks are drawn in Section VI.

II. Model-Based Fault Detection and Isolation: Problem Setup

Model-based fault detection and isolation targets the identification of the health status $\boldsymbol{k} = \left[k_1, ..., k_{n_k}\right]$ of the system as the combination of n_k faults parameters $\boldsymbol{k}$ that minimizes the discrepancy δ between the output signal of the real system $\boldsymbol{y}$ and the signal computed with a numerical model of the system $\boldsymbol{y}_M$. Accordingly, the FDI procedure is formalized as an inverse problem:

$$\boldsymbol{k}^* = \operatorname*{arg\,min}_{\boldsymbol{k} \in \mathcal{K}} \delta(\boldsymbol{k}, \boldsymbol{x}) \tag{1}$$

where $\delta(\boldsymbol{k}, \boldsymbol{x}) = ||\boldsymbol{y}(\boldsymbol{k}^*, \boldsymbol{x}) - \boldsymbol{y}_M(\boldsymbol{k}, \boldsymbol{x})||$, and $\boldsymbol{k}^*$ is the actual health status affecting the system.

The output signal $\boldsymbol{y}$ is ideally sensitive to faults and insensitive to other input, and it is generally high-dimensional and unpractical to store and process for rapid diagnostic procedures. In addition, the computation of an accurate monitoring signal $\boldsymbol{y}_M$ requires the simulation of the system behaviour through expensive numerical models or real-world experiments. Those high-fidelity representations further impact the computational burden of monitoring and diagnosis the health status of complex dynamical system.

III. Multifidelity Fault Detection and Isolation

The proposed methodology combines two constitutive phases: the first optimizes the informative content of the diagnostic signals minimizing the computational burden associated with their management through the two-stage optimal compression strategy (Section III.A); the second efficiently includes high-fidelity models to support the accurate inference of incipient faults through a multifidelity Bayesian scheme for inference (Section III.B). The original combination of those elements permits to address the limitations of standard model-based FDI techniques, and enables the efficient inference of multiphysics and multimodal incipient faults of complex systems.

A. Two-Stage Optimal Informative Compression

The two-stage optimal compression technique is performed during the setting process and consists on two main ingredients: i) the Dynamic Mode Decomposition (DMD) identifies a set of dominant coherent structures of the system behaviour, and ii) a Self Organizing Map (SOM) projects these structures into a lower-dimensional space and computes an efficient encoding map that synthesizes the overall dynamic of the system. The procedure is inspired by the two-stage compression proposed by Mainini [14] and Mainini and Willcox [15] where Proper Orthogonal Decomposition and Self Organizing Maps jointly identify the optimal sensor placement in structural health monitoring applications, and applied by Berri et al. [16] for the FDI of aircraft electromechanical actuators.

1. Dynamic Mode Decomposition

The first stage of our compression strategy adopts the Dynamic Mode Decomposition (DMD) technique to extract the dynamical features of the system in the form of dynamic modes [17, 18]. From a general perspective, a dynamical system affected by damages could be considered as a non-linear system ψ whose output signal $y(k,x) \in \mathbb{R}^{n_e}$ is sensitive to the health status k of the system and to the measurement locations x. DMD seeks to identify the dynamical properties of this system as the dominant eigenvalues and eigenvectors of the informative matrix $\tilde{A} \in \mathbb{R}^{n_e \times n_e}$ such that:

$$\tilde{A}\tilde{Y} = \tilde{Y}' \tag{2}$$

where

$$\tilde{Y} = \begin{bmatrix} \tilde{y}^{(L)}(k_0,x) & \tilde{y}^{(L)}(k_1,x) & ... & \tilde{y}^{(L)}(k_{n_s-1},x) \end{bmatrix} \in \mathbb{R}^{n_e \times n_s}$$

$$\tilde{Y}' = \begin{bmatrix} \tilde{y}^{(L)}(k_1,x) & \tilde{y}^{(L)}(k_2,x) & ... & \tilde{y}^{(L)}(k_{n_s},x) \end{bmatrix} \in \mathbb{R}^{n_e \times n_s}$$

are the snapshot matrices. Those snapshots are computed offline through an high-fidelity representation of the system $\psi^{(L)}$, and collect a series of n_s paired high-fidelity output signals $\tilde{y}^{(L)}(k_{j-1},x)$ and $\tilde{y}^{(L)}(k_j,x)$ computed for incipient fault conditions $\{k_j\}_{j=1}^{j=n_s}$ assembled via scaled Latin hypercube sampling scheme [16].

The computation of the informative matrix $\tilde{A}$ is usually unfeasible: the direct solution of Equation (2) is hampered by the significant computational cost required for large snapshot matrices – frequently encountered in many real-world applications in science and engineering. A popular approach to overcome this issue adopts the Singular Value Decomposition (SVD) technique [19] to identify a set of $n_w << n_s$ informative modes $B \in \mathbb{C}^{n_e \times n_s}$. This permits to retain a large fraction of information embedded in the snapshot matrices, and quantifies this informative content as the cumulative sum $\sum_{i=1}^{n_w} \lambda_i / \sum_{i=1}^{n_s} \lambda_i$ of the eigenvalues λ associated to the considered modes. This allows to project the snapshot matrices $\tilde{Y}$ and $\tilde{Y}'$ onto the first n_w modes, and compute the matrices Y and Y':

$$Y = B^*\tilde{Y} \in \mathbb{R}^{n_w \times n_s} , \quad Y' = B^*\tilde{Y}' \in \mathbb{R}^{n_w \times n_s} \tag{3}$$

where B^* is the Hermitian transpose of B. Thus, the DMD problem (Equation (2)) becomes manageable and the information matrix can be computed as follows:

$$A = Y'Y^+ \tag{4}$$

where Y^+ is the Moore-Penrose pseudoinverse of Y. The eigendecomposition of the informative matrix A yields the dominant eigenvalues and eigenvectors that encode the fundamental properties of the underlying dynamical system in the form of dynamic modes $\Upsilon = [v_1,...,v_{n_w}]$.

2. Self-Organizing Map

In the second stage of compression, a Self Organizing Map (SOM) projects the DMD modes Υ into a lower-dimensional space, and computes an efficient compression map of the output signal $\hat{y}(k,\hat{x})$ that preserves the topological properties of those modes. This representation retains only the highly informative elements $n_w << n_e$ of the output signal, and is used in the online phase to alleviate the computational burden of the FDI procedure.

Self-organizing map (SOM) is a competitive artificial neural network trained with unsupervised learning paradigms to produce a low-dimensional representation of the input space of the training samples [20, 21]. Considering a non-linear damaged system ψ, the training set T consists of the dynamic modes of the system Υ and the measurement locations x of the output signal:

$$T = [x, v_1, ..., v_{n_w}] \tag{5}$$

During the SOM training process, each row τ_i of T is presented to the network and the node that shows greater similarity to this input is selected to be the winner. This winning node is updated towards the input vector, and the other nodes are influenced according to their topological distances from the winner. In particular, the winning neuron is selected as the one that minimizes the distance between the associated weight vector w_l and the current training point τ_i:

$$l = \arg\min_j \left(||\tau_i - w_j|| \right) \tag{6}$$

where $||\cdot||$ denotes the L2 norm.

In the final layout of a trained SOM, adjacent nodes have an high similarity to each other and are dissimilar to nodes that are located far apart. This trained net represents a non-linear projection of the training set T to the lower dimensional space of the neurons, and the weight vectors in the input space encode representative vectors for clusters of self-similar points [14, 15, 22]. This permits to extract the latent structure of the training input and compute the efficient compression map $\hat{y}(k,\hat{x})$.

B. Multifidelity Bayesian Scheme for Damage Inference

The informative map $\hat{y}(k,\hat{x})$ reduces the dimensionality of the FDI problem:

$$k^* = \arg\min_{k \in \mathcal{K}} \delta(k,\hat{x}) \tag{7}$$

where $\delta(k,\hat{x}) = ||\hat{y}(k^*,\hat{x}) - \hat{y_M}(k,\hat{x})||$ is now evaluated only for the n_w informative elements of the reference compressed signal $\hat{y}$ and monitoring compressed output $\hat{y_M}$. To address this inverse problem, we adopt a multifidelity Bayesian scheme to leverage queries of the discrepancy function $[\delta^{(1)}, \delta^{(2)}, ..., \delta^{(L)}]$ at different levels of fidelity and accelerate the inference of the damages affecting the system [23–26]. Multifidelity Bayesian frameworks build onto the Bayesian scheme [27–29] and have been explored in the context of aerospace design optimization [30–32] where it has been observed major accelerations in the identification of optimal design solutions.

The damage inference procedure is performed dynamically online through an iterative process and adopts two key elements: the multifidelity surrogate model and the multifidelity acquisition function. The surrogate approximates the discrepancy function based on collected information, and provides a predictive framework that synthesizes the data from multifidelity models into a unique emulator. At each iteration, the acquisition function informed by this predictive distribution is maximized to select the damage configuration that is likely to actually affect the system together with the associated fidelity of the representation to query. Meanwhile, the new observation is used to update the posterior distribution of the emulator, and the above process is repeated until a convergence metric is met.

1. Multifidelity Gaussian Process

Our multifidelity FDI strategy adopts the Gaussian process regression to compute the surrogate model of the discrepancy function $\delta^{(l)}(k)$ at different levels of fidelity, and predicts its distribution over the faults domain $\mathcal{K}$. Gaussian process (GP) regression constructs a non-parametric kernel-based probabilistic surrogate based on the observations of the discrepancy at previous evaluated damage configurations, and quantifies the uncertainty associated with this approximation [33, 34]. This results in a predictive framework completely specified by its mean function $\mu(k) : \mathcal{K} \rightarrow \mathbb{R}$ and kernel function $\kappa(k,k') : \mathcal{K} \times \mathcal{K} \rightarrow \mathbb{R}$.

In the multifidelity scenario, the GP regression synthesizes the simulations from the models at different levels of fidelity $[\delta^{(1)}, \delta^{(2)}, ..., \delta^{(L)}]$ into a unique predictive framework. The Multifidelity Gaussian Process (MFGP) is

formalized through an autoregressive relation between adjacent levels of fidelity. Let us assume we have collected paired input/output observations in the dataset $\mathscr{D}_N = \{\boldsymbol{k}_n, f^{(l_n)}(\boldsymbol{k}_n), l_n\}_{n=1}^N$, where the output $\boldsymbol{f} = \{f^{(l_n)}(\boldsymbol{k}_n)\}_{n=1}^N$ is normally distributed given $\boldsymbol{\Delta} = \{\delta_n^{(l_n)}\}_{n=1}^N$:

$$\boldsymbol{f} \mid \boldsymbol{\Delta}, \sigma_\varepsilon^2 \sim \mathcal{N}(\boldsymbol{\Delta}, \sigma_\varepsilon^2 \boldsymbol{I}) \tag{8}$$

assuming the same variance of the measurement noise σ_ε^2 for each level of fidelity. The MFGP relies on the linear autoregressive information fusion proposed by Kennedy and O'Hagan to approximate the discrepancy function [35]. This scheme assigns a GP prior to the lower fidelity model $\delta^{(1)} \sim GP(0, \kappa_1(\mathbf{k}, \mathbf{k}'))$ with mean function $\mu^{(l)} = 0$ and kernel function $\kappa_1(\mathbf{k}, \mathbf{k}')$, and defines recursively the higher-fidelity levels as follows:

$$\delta^{(l)} = \rho^{(l-1)}(\boldsymbol{k})\delta^{(l-1)}(\mathbf{k}) + \gamma^{(l)}(\mathbf{k}) \quad l = 2, ..., L \tag{9}$$

where the scale factor $\rho^{(l-1)}(\boldsymbol{k})$ models the correlation between the outputs of adjacent levels of fidelity, and $\gamma^{(l)} \sim GP(0, \kappa^{(l)}(\mathbf{k}, \mathbf{k}'))$ represents the modeling discrepancy between two adjacent levels of fidelity as a Gaussian process with mean function $\mu^{(l)} = 0$ and kernel function $\kappa^{(l)}(\mathbf{k}, \mathbf{k}')$.

Following the Bayesian inference principle, the MFGP regression combines the prior belief about the objective $P(\delta^{(l)})$ with the likelihood function $P(\mathscr{D}_N | \delta^{(l)})$, and computes the updated posterior distribution of the discrepancy function $P(\delta^{(l)} | \mathscr{D}_N) \propto P(\mathscr{D}_N | \delta^{(l)}) P(\delta^{(l)})$. This multifidelity posterior is a Gaussian process completely specified by its mean function $\mu^{(l)}$ and variance function $\sigma^{2(l)}$:

$$\mu^{(l)}(\mathbf{k}) = \kappa_N^{(l)}(\mathbf{k})^T (\boldsymbol{K} + \sigma_\varepsilon \boldsymbol{I})^{-1} \boldsymbol{f} \tag{10}$$

$$\sigma^{2(l)}(\mathbf{k}) = \kappa((\mathbf{k}, l), (\mathbf{k}, l)) - \kappa_N^{(l)}(\mathbf{k})^T (\boldsymbol{K} + \sigma_\varepsilon \boldsymbol{I})^{-1} \kappa_N^{(l)}(\mathbf{k}) \tag{11}$$

where $\kappa_N^{(l)}$ is defined as $\kappa_N(\mathbf{k}) \doteq (\kappa((\mathbf{k}, l), (\mathbf{k}_1, l_1)), \cdots, \kappa((\mathbf{k}, l), (\mathbf{k}_N, l_N)))$, and $\boldsymbol{K}$ is the kernel matrix defined as follows:

$$\boldsymbol{K} = \begin{pmatrix} \kappa^{(l-1)}(\boldsymbol{k}, \boldsymbol{k}') \boldsymbol{K}^{(l-1)} & \rho \, \kappa^{(l-1)}(\boldsymbol{k}, \boldsymbol{k}') \boldsymbol{K}^{(l-1)} \\ \rho \, \kappa^{(l-1)}(\boldsymbol{k}, \boldsymbol{k}') \boldsymbol{K}^{(l-1)} & \rho^2 \kappa^{(l-1)}(\boldsymbol{k}, \boldsymbol{k}') \boldsymbol{K}^{(l-1)} + \kappa^{(l)}(\boldsymbol{k}, \boldsymbol{k}') \boldsymbol{K}^{(l)} \end{pmatrix} \tag{12}$$

where $\boldsymbol{K}^{(l-1)}(i, j) = \kappa((\boldsymbol{k}_i, l-1), (\boldsymbol{k}_j, l-1))$ and $\boldsymbol{K}^{(l)}(i, j) = \kappa((\boldsymbol{k}_i, l), (\boldsymbol{k}_j, l))$.

The mean function $\mu^{(l)}(\mathbf{k})$ represents the prediction of the discrepancy $\delta^{(l)}(\boldsymbol{k})$ over the possible combinations of fault parameters in the domain $\mathscr{K}$, and $\sigma^{2(l)}(\mathbf{k})$ quantifies the associated uncertainty. In addition, this predictive framework shows a potential form of intrinsic reliability through the estimated uncertainty $\sigma^{2(l)}$: the discrepancy function has bounded norm in the reproducing kernel Hilbert space induced by the kernel function [36]. Thus, the discrepancy is characterized by reliable confidence intervals that determine the overall reliability of the multifidelity surrogate model. Within the multifidelity FDI procedure, this posterior distribution informs and assists the multifidelity acquisition function during the inference stage.

2. Multifidelity Acquisition Function

The multifidelity acquisition function $U(\boldsymbol{k}, l) : \mathscr{K} \to \mathbb{R}^+$ measures the improvement in terms of accuracy of the damages inference, and wisely uses the computational resources during the search with a continuous trade-off between the exploration of uncertain locations of the faults domain and exploitation toward the believed health status of the system. Different formulations of the acquisition function can be used in our framework: those include multifidelity expected improvement (MFEI) [37], multifidelity entropy search (MFES) [38], multifidelity max-value entropy search (MFMES) [39], variable-fidelity probability of improvement (VFPI) [40] and Non-Myopic MFEI (NM-MFEI) [41], which all implement different measures of the evaluation reward. In this work, we adopt the most popular multifidelity expected improvement [30, 42] (Section III.B.3), and the non-myopic acquisition function (Section III.B.4).

3. Multifidelity Expected Improvement

Given a new fault combination k and n associated level of fidelity l at which the condition is evaluated, the multifidelity expected improvement acquisition function quantifies the improvement in expectation with respect to the *best* combination of damages $\hat{k}^*$ computed so far:

$$U_{MFEI}(k,l) = U_{EI}(k)\alpha_1(k,l)\alpha_2(k,l)\alpha_3(l) \tag{13}$$

where $U_{EI}(k)$ is the expected improvement acquisition function [43]:

$$U_{EI}(k) = \sigma^{(L)}(k)(I(k)\Phi(I(k))) + \mathcal{N}(I(k);0,1) \tag{14}$$

where $I(k) = (\delta^{(L)}(\hat{k}^*) - \mu^{(L)}(k))/\sigma^{(L)}(k)$ is the high-fidelity predicted improvement, and $\Phi(\cdot)$ is the cumulative distribution function of a standard normal distribution.

The utility functions α_1, α_2 and α_3 support the search procedure, and balance the selection of the appropriate level of fidelity to evaluate the generic k:

$$\alpha_1(k,l) = corr\left[\delta^{(l)}, \delta^{(L)}\right] = \frac{\kappa((k,l),(k,L))}{\sqrt{\sigma^{2(l)}\sigma^{2(L)}}} \tag{15}$$

$$\alpha_2(k,l) = 1 - \frac{\sigma_\varepsilon}{\sqrt{\sigma^{2(l)}(k) + \sigma_\varepsilon^2}} \tag{16}$$

$$\alpha_3(l) = \frac{\lambda^{(L)}}{\lambda^{(l)}}. \tag{17}$$

α_1 pursues the adoption of the high-fidelity model when lower-fidelity representations might provide an unreliable estimate of the health status of the system. This awareness is reflected decreasing the MFEI through the posterior correlation coefficient if the discrepancy computed with the l-th level of fidelity is inaccurate for a specific damage configuration k. α_2 contains the over-exploration of regions of the faults domain $\mathcal{K}$ where the uncertainty of the surrogate model has been already reduced with previous observations. This utility function reflects the stochastic nature of the objective function and measures the reduction of the surrogate uncertainty achieved through new observations of the discrepancy function $\delta^{(l)}(k)$. α_3 includes the computational cost $\lambda^{(l)}$ required to compute the l-th representation of the discrepancy compared to the high-fidelity burden $\lambda^{(L)}$. This term balances the contribution of α_1, and solicits lower-fidelity queries when a similar accuracy is obtained evaluating the health status of the system with the high-fidelity model.

4. Non-Myopic Multifidelity Expected Improvement

The non-myopic MFEI acquisition function measures the informative gains over future iterations given by a potential health condition of the system k and associated level of fidelity l. This search scheme is obtained formalizing an optimal policy as a sequence of decisions that maximizes the cumulative reward over two steps ahead [41]:

$$U_{NM}(k_{i+2}, l_{i+2}) = U_{MFEI}(k_{i+1}, l_{i+1}) + \mathbb{E}\left[\max\left(U_{MFEI}(k_{i+2}, l_{i+2})\right)\right] \tag{18}$$

where i is the current iteration of the FDI procedure. The non-myopic acquisition function involves intractable nested expectations and maximizations that require the prediction of future optimization scenario not directly available at the current iteration. We define a Monte Carlo technique to robustly estimate the prediction $\mu_{i+1}^{(l)}$ and uncertainty $\sigma_{i+1}^{(l)}$ of the multifidelity surrogate model at the first step ahead [44]:

$$\mu_{i+1}^{(l)}(\mathbf{k}) = \mu_i^{(l)}(\mathbf{k}) + H_i^{(l)}(\mathbf{k})Z \tag{19}$$

$$\sigma_{i+1}^{(l)}(\mathbf{k}) = \sigma_i^{(l)}(\mathbf{k}) - H_i^{(l)}(\mathbf{k})H_i^{(l)}(\mathbf{k})^T \tag{20}$$

where $H_i^{(l)}(\mathbf{k}) = \kappa_i^{(l)}(\mathbf{k})C_i^{(l)-1}(\mathbf{k})$ and $C^{(l)}$ is the Cholesky decomposition of the kernel matrix $K(k_i, k_j)$. This numerical approach samples many replications of an independent standard normal random variable Z, and approximates U_{NM} averaging many realizations obtained through the predictive framework updated at the first step ahead (Equation (19) and Equation (20))
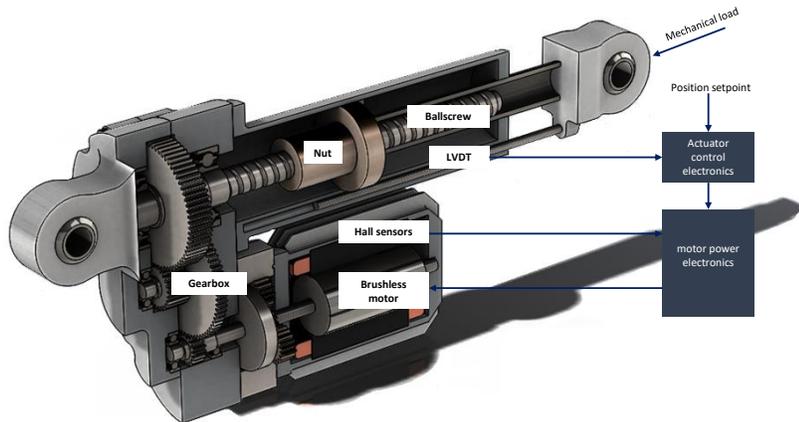
6

Fig. 1   An aerospace electromechanical actuator

IV. Aerospace Electromechanical Actuator (EMA)

We demonstrate our methodology on the test case of fault detection and identification for an aerospace Electrome-chanical Actuator (EMA). These devices convert electrical energy into mechanical motion, and are widely employed to power secondary flight controls, as well as utilities such as landing gear and cargo bay doors, weapons systems, or gimbals for electro-optics sensors. The adoption of EMAs for applications traditionally reserved to hydraulic systems, in particular primary flight controls, is a key step for enabling more-electric and all-electric aircraft designs, with significant benefit in terms of carbon footprint and operating costs [1, 11–13]. The progressive switch to EMA based flight control systems is currently underway in upcoming platforms, and will be facilitated by the adoption of reliable fault detection strategies. The common subsystems of an aerospace EMA (Figure 1) includes a brushless motor with its power electronics, and a mechanical transmission with a reduction gearbox and a screw device to convert rotary motion to linear translation of the output. A network of sensors measures positions, speeds, temperatures and electrical parameters to inform the control electronics and close the feedback loops.

FDI for Aerospace EMAs is a particularly challenging task as the monitored system combines multi-physical behaviors involving the interaction between electrical, mechanical and thermal subsystems, which can exhibit highly nonlinear behaviors under different conditions. As a consequence, EMAs may show multiple fault modes that can interact with each other through causal relationships (i.e. an initial fault can propagate to other components) yielding to nonlinear combinations of effects on the actuator's performances. Additional challenges to FDI are posed by the harsh environment in which aerospace actuators are required to operate: EMAs are often exposed to extreme temperature changes, high vibration and acceleration levels, and electromagnetic disturbances, all of which can hamper the acquisition of accurate and reliable sensor data.

We employ as a case study an EMA based on a BrushLess Direct Current (BLDC) motor, installed as an elevator flight control. The health condition of the system is encoded in $k \in \mathbb{R}^7$. Four different failure modes are considered, namely friction (k_1) and backlash (k_2) increases, partial short circuit of the three stator windings ($k_{3,4,5}$ respectively) and rotor eccentricity ($k_{6,7}$ for the eccentricity amplitude and phase). These failure modes are selected for their comparatively high probability of occurrence and criticality [45]. For each element of k, a null value represents a nominal condition without faults, while a unit value is a full failure state. The variable monitored for the FDI task is the equivalent DC stator current $I = \frac{1}{2}(|i_A| + |i_B| + |i_C|)\text{sign}(T_m)$, where T_m is the motor torque and $i_{A,B,C}$ are the stator phase currents. This variable is sensitive to faults and is already measured to close the torque feedback loop. We use two physics-based numerical models of the EMA at different levels of fidelity to demonstrate the capabilities of our multifidelity FDI algorithm. In addition, we employ the data acquired from a real-world EMA test-bench to validate the efficiency of the proposed methodology. The following sections briefly describe the two numerical models and the physical test-bench of the EMA. Further details are available from [46, 47].
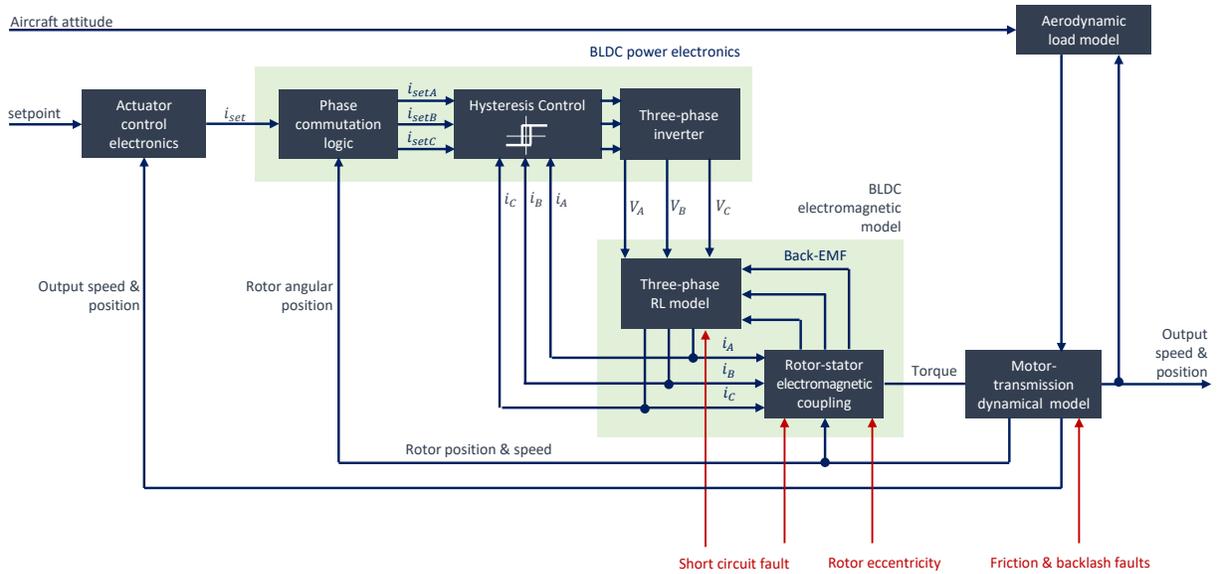
Fig. 2 Block diagram of the HF EMA model

A. High Fidelity (HF) model

The High Fidelity (HF) model of the actuator is a detailed, physics-based emulator of the EMA's dynamical behavior. The model has a high accuracy in simulating the response of a physical system, as validated experimentally in [48]. Figure 2 shows the block diagram of the high-fidelity models. At the core of the HF model is a three-phase simulation of the stator currents, including the hysteresis closed-loop current control and the resistive-inductive (RL) model of the stator coils. The electromagnetic coupling between the wound stator and the permanent magnet rotor is mapped as a function of the rotor angular position and magnetic flux that concatenates with the stator coils. The magnetic flux time derivative is leveraged to evaluate both the back-EMF and the torque generated by the motor. The magnetic model is sensitive to asymmetries in the air gap distribution and to unbalances in the windings, therefore faults like rotor eccentricity and partial short circuits of the stator can be simulated directly.

The mechanical transmission is modelled as a second order dyamical system, that includes the simulation of several nonlinear effects, namely: backlash, dry friction, mechanical endstops, and the finite stiffness of load-carrying components. The mechanical load on the actuator is simulated through the linearized longitudinal model of the F-16 jet aircraft proposed by Stevens [49]. Stator currents i_A, i_B and i_C are measured to close the current/torque control loop; the velocity and position loops rely on three Hall effect sensors on the motor shaft and a linear displacement sensor (LVDT) on the actuator output, respectively. The current loop is managed by three individual hysteresis controllers, one for each phase; the position and velocity loops feature Proportional-Integral-Derivative (PID) regulators with full anti-windup, derivative filtering and dead-band functions to inhibit limit cycles.

We utilize this HF model as an emulator of a real-world actuator to evaluate the proposed FDI strategy and gather ground truth data for our two-step compression methodology. However, the high computational cost required to estimate the dynamic of the EMA system is nearly two orders of magnitude higher than the simulated time interval, making the FDI task with the high-fidelity model alone impractical with limited computational resources. As a result, we aim to develop a low-fidelity model of the EMA system that introduces approximations to alleviate the computational burden while maintaining an acceptable level of accuracy in simulating the actuator's dynamics.

B. Low Fidelity (LF) model

The Low Fidelity model of the actuator introduces simplifications to the physical representation of the EMA in order to reduce the computational cost in evaluation while retaining an acceptable accuracy. The block diagram of the LF model is shown in Figure 3. The main simplification with respect to the HF model is the replacement of the three-phase RL stator simulation with a single-phase equation:
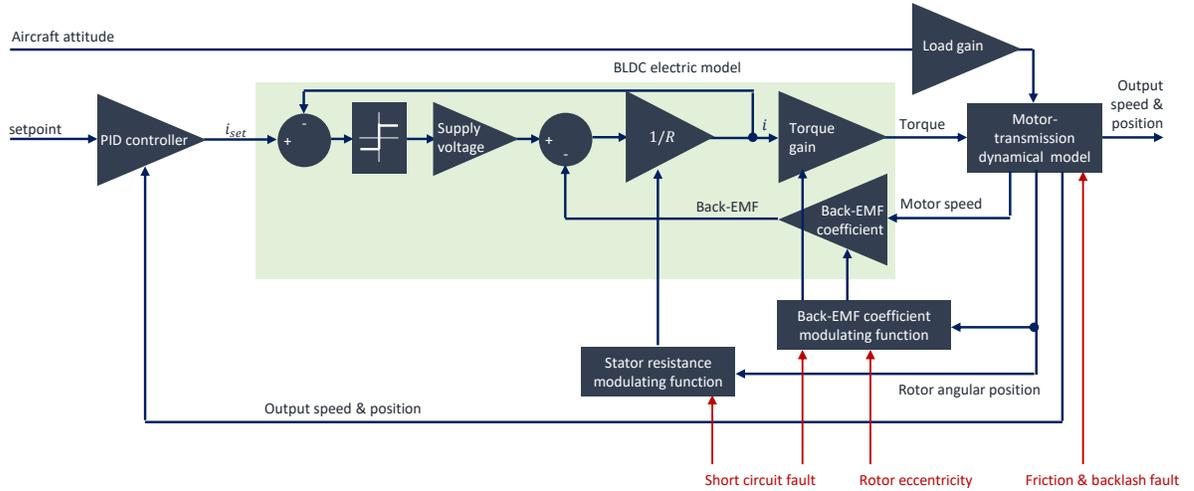
8

Fig. 3   Block diagram of the LF EMA model

$$V = RI + \kappa_v \omega \tag{21}$$

where κ_v is the motor's back-EMF coefficient and ω is the rotor's angular speed. This approach enables to speed up computations significantly, as the stator circuit is pre-solved and does not require to run an iterative solver at each timestep. This approach requires to introduce the sensitivity to fault modes empirically through modulating functions for the motor parameters, as proposed by Berri et al. [50]. In addition, the control logic only includes a linear PID for the speed and position loops, and a simplified hysteresis controller – consisting in a single sign function – manages the current loop. The aerodynamic load is estimated from the aircraft attitude with a proportional gain, neglecting the longitudinal dynamics of the entire vehicle. In this work, the LF model is used alongside with the HF one as a source of information to compute the monitoring current signal of the EMA system.

C. Physical test bench

The proposed FDI strategy is validated experimentally with data from a real-world EMA test-bench capable to simulate the presence of mechanical faults in the transmission. The setup, shown in Figure 4, includes a permanent magnet brushless motor connected to a planetary reduction gearbox. The motor is driven by a current-controlled, 400 V three-phase inverter. A separate 24 VDC bus drives the control logic. A pair of high resolution encoders measure the position of the motor shaft and the position of the gearbox output shaft: the former is used for phase commutation and speed feedback while the latter closes the position control loop. A repeatable mechanical load is provided by a servo-actuated brake module, whose torque is measured by a loadcell and controlled in closed loop. This permits to simulate different load profiles and include the effect of a friction increase fault. Moreover, the last gear pair driving the output shaft is adjustable, and allows to simulate the backlash fault through a controlled variation of the mechanical play. Acquisitions from the test bench were initially used to validate the HF and LF models in nominal conditions and in presence of mechanical faults [51]. In addition, the measurements of current signals from the EMA test-bench are used as the reference signal to validate the performance of the proposed multifidelity FDI strategy.

V. Experiments and Discussion

In this section, we illustrate and discuss the results achieved with the proposed multifidelity FDI (MFDI) approach for the EMA diagnostic problem (Section IV). We compare our framework with the state-of-the-art Efficient Global Optimization (EGO) algorithm, a popular Bayesian algorithm where the expected improvement works as the acquisition function and only the high-fidelity EMA model is available during the FDI procedure [43].

For our method, we assemble offline a reference dataset of the EMA current signal over 100 incipient fault conditions, and use the two-stage compression strategy (Section III.A) to compute the informative map of the EMA on these reference information. Online, the multifidelity Bayesian procedure (Section III.B) implements both the multifidelity
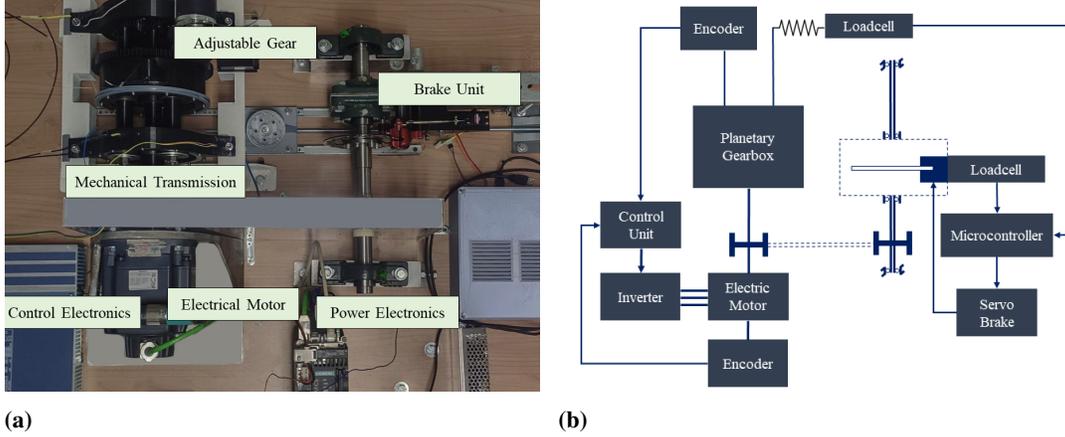
Fig. 4   (a) EMA test-bench and (b) the corresponding block diagram

expected improvement (MFEI) and the non-myopic MFEI (NM-MFEI). We conduct numerical and physical experimental campaigns to assess the capabilities of our framework. In the numerical experiments, the high-fidelity EMA model computes the reference current signal and is available jointly with the low-fidelity model to compute the monitoring current signal during the FDI procedure. In the physical tests, the reference current signal is measured through the EMA test-bench, and both the high- and low-fidelity EMA models are used to simulate the monitoring output. All the algorithms are implemented in the Matlab environment and the experiments are conducted on a laptop PC with Intel Core i7-6700HQ and 32GB memory.

The FDI performance are evaluated using two assessment metrics: the percentage relative inference error $e(k_i)$ of the k_i fault, and the minimum of the discrepancy function δ^* between the reference and monitoring signal:

$$e(k_i) = \frac{||k_i^* - \widetilde{k}_i||}{k_i^*} \cdot 100 \tag{22}$$

$$\delta^* = \min(\delta(\boldsymbol{k}^*, \hat{\boldsymbol{x}})) \tag{23}$$

where k_i^* is the actual damage affecting the EMA system and $\widetilde{k}_i$ is the damage inferred by the FDI algorithm. For both numerical and physical experiments, these metrics are measured over a statistics of, respectively, 50 and 10 different incipient damage conditions sampled through a scaled Latin hypercube scheme [16]. This sampling procedure increases the probability distribution of damages near the nominal condition, and expands the amount of small incipient faults without completely excluding more serious damages. The goal is to investigate the capabilities of the FDI algorithm to identify the health status of the EMA system before the damages become severe – and easily assessed. In the following, the outcomes of the experimental campaigns are reported in terms of median values of the assessment metrics together with the statistics in between the 25-th and 75-th percentiles.

Figure 5 and Figure 6 show the results of the competing algorithms for the numerical and physical experiments, respectively. We make the following empirical observations: i) our MFDI algorithm consistently converges much faster than the baseline EGO algorithm with all the formulations of the multifidelity acquisition function – both MFEI and NM-MFEI. In particular, the multifidelity paradigm achieves remarkable accelerations and reduces the identification time by more than one order of magnitude. ii) The rate of convergence of NM-MFEI is moderately higher that the MFEI acquisition function. However, in all the experimental campaign the proposed MFDI outperforms the single-fidelity EGO algorithm. iii) The proposed algorithm provides the exact inference of the incipient faults affecting the EMA system ($e(k_i) = 0$). These results demonstrate and validate the performance of our framework, which provides a fast and robust inference of incipient multiphysics and multimodal faults affecting the EMA. In numerical experiments, the average runtime of NM-MFEI and MFEI is within 32 seconds and 39 seconds, respectively, which is notably lower if compared with the 691 seconds runtime of EGO. Similarly, the diagnosis of the real-world EMA takes 26 seconds for NM-MFEI and 42 seconds for MFEI on average, while EGO increases the duration of the FDI process to 273 seconds.

The convergence of the minimum discrepancy in both the settings is not strictly related to the continuous decrease of the inference error over the runtime. This can be justified with the ill-posedness of the EMA inverse problem: the FDI
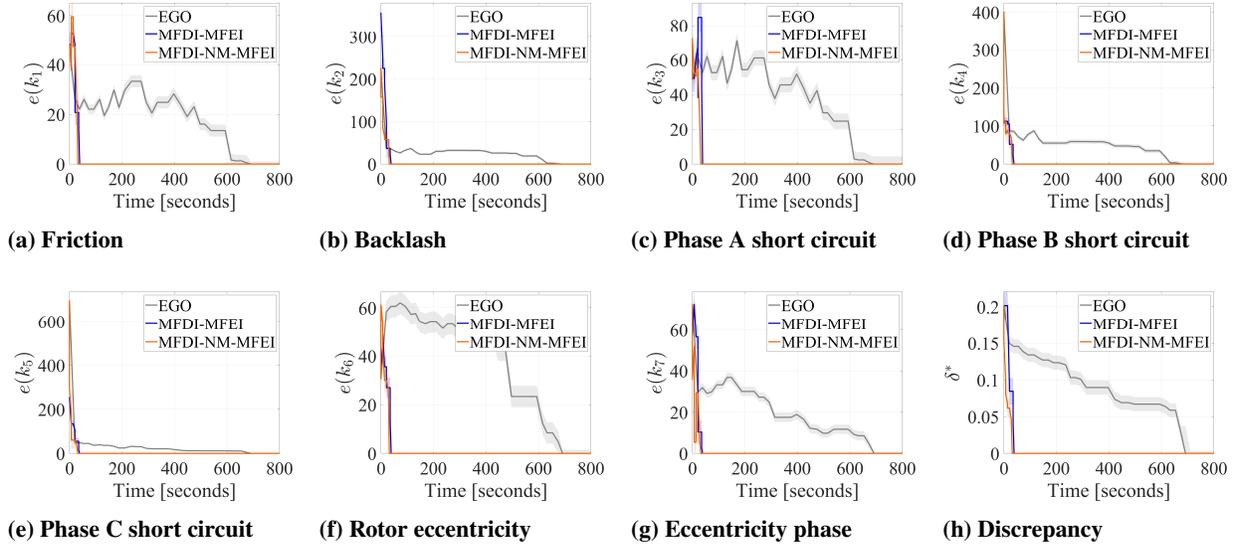
Fig. 5   Results of our MFDI algorithm and EGO on numerical experiments.
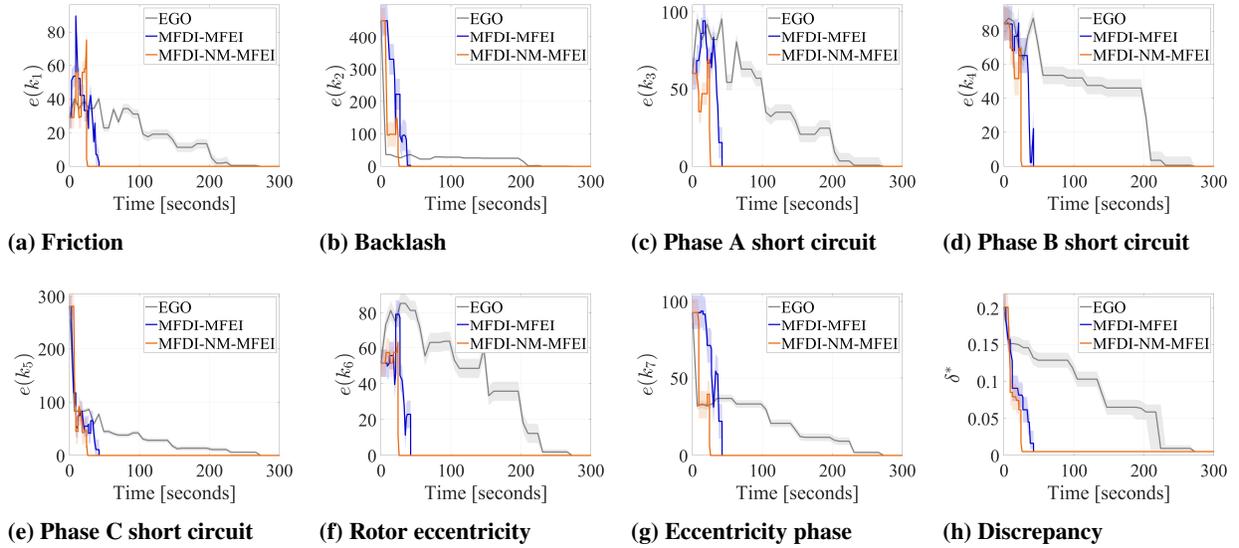

Fig. 6   Results of our MFDI algorithm and EGO on physical experiments.

procedure is subject to instability caused by the joint decrease of the discrepancy function and increase of the inference error. As highlighted by [52], this behaviour results from the opposite effects of heterogeneous damages on the EMA dynamics: the increase of the mechanical friction k_1 decreases the actuation speed while the increase of the partial short circuit $k_{3:5}$ increases the speed of the motor shaft. As a consequence, the discrepancy function is characterized by a strong multimodality that stresses the FDI framework.

The remarkable accelerations achieved in the experimental campaigns demonstrate and validate the efficiency and robustness of our multifidelity FDI framework even in presence of incipient faults and marked multimodality. These outcomes emerge from the original combination of two distinguishing features: i) the optimal two-stage compression reduces the signals into highly informative representations that reduces the dimensionality of the FDI problem, and ii) the multifidelity Bayesian scheme for inference wisely queries high-fidelity models to enhance the identification procedure while contains the overall computational expenditure through low-fidelity evaluations.

11

VI. Concluding Remarks

The proposed multifidelity fault detection and identification (FDI) framework permits to accelerate the identification of multiphysics and multimodal incipient faults of complex systems. Our algorithm relies on the original combination of a two-stage optimal compression strategy to reduce the dimensionality of the diagnostic signals, and a multifidelity Bayesian scheme to infer incipient failure modes through the combination of multiple models with variable fidelities and costs. We demonstrate and validate the proposed methodology for the FDI of an aerospace electromechanical actuator affected by incipient mechanical and electrical faults. We conducted both numerical and physical experiments where our multifidelity scheme is compared with the standard single-fidelity efficient global optimization algorithm.

The results show that our multifidelity FDI outperforms standard single-fidelity algorithms in terms of accuracy and acceleration of the inference. In particular, numerical experiments reveal that the proposed methodology equipped with the non-myopic scheme achieves the exact identification of the EMA health status 95.4 % faster than the single-fidelity approach. The physical experiments confirm and validate the efficiency of the proposed framework: our strategy identifies with the non-myopic search the exact damage condition of the real-world EMA reducing the computational cost by 90.5 % if compared with the single-fidelity algorithm. The remarkable accelerations and accuracy of the FDI procedure are enabled by the combination of the efficient compression of the diagnostic signals through the encoding map, and the effective use of high-fidelity responses to accurately identify multiphysics damages. These achievements encourage the adoption of multifidelity FDI schemes as enabling techniques to monitor the health status of novel technologies on board of the next generation of aircraft.

Acknowledgments

References

[1] Schäfer, A. W., Barrett, S. R., Doyme, K., Dray, L. M., Gnadt, A. R., Self, R., O'Sullivan, A., Synodinos, A. P., and Torija, A. J., "Technological, economic and environmental prospects of all-electric aircraft," *Nature Energy*, Vol. 4, No. 2, 2019, pp. 160–166. https://doi.org/https://doi.org/10.1038/s41560-018-0294-x.

[2] Afonso, F., Sohst, M., Diogo, C. M., Rodrigues, S. S., Ferreira, A., Ribeiro, I., Marques, R., Rego, F. F., Sohouli, A., Portugal-Pereira, J., et al., "Strategies towards a more sustainable aviation: A systematic review," *Progress in Aerospace Sciences*, Vol. 137, 2023, p. 100878. https://doi.org/https://doi.org/10.1016/j.paerosci.2022.100878.

[3] Ranasinghe, K., Sabatini, R., Gardi, A., Bijjahalli, S., Kapoor, R., Fahey, T., and Thangavel, K., "Advances in Integrated System Health Management for mission-essential and safety-critical aerospace applications," *Progress in Aerospace Sciences*, Vol. 128, 2022, p. 100758. https://doi.org/https://doi.org/10.1016/j.paerosci.2021.100758.

[4] Isermann, R., "Model-based fault-detection and diagnosis–status and applications," *Annual Reviews in control*, Vol. 29, No. 1, 2005, pp. 71–85. https://doi.org/https://doi.org/10.1016/s1474-6670(17)32149-3.

[5] Zolghadri, A., "Advanced model-based FDIR techniques for aerospace systems: Today challenges and opportunities," *Progress in Aerospace Sciences*, Vol. 53, 2012, pp. 18–29. https://doi.org/https://doi.org/10.1016/j.paerosci.2012.02.004.

[6] Marzat, J., Piet-Lahanier, H., Damongeot, F., and Walter, E., "Model-based fault diagnosis for aerospace systems: a survey," *Proceedings of the Institution of Mechanical Engineers, Part G: Journal of aerospace engineering*, Vol. 226, No. 10, 2012, pp. 1329–1360. https://doi.org/https://doi.org/10.1177/0954410011421717.

[7] Kolcio, K. O., "Model-based fault detection and isolation system for increased autonomy," *AIAA SPACE 2016*, American Institute of Aeronautics and Astronautics, 2016, p. 5225. https://doi.org/https://doi.org/10.2514/6.2016-5225.

[8] Omata, N., Tsutsumi, S., Abe, M., Satoh, D., Hashimoto, T., Sato, M., and Kimura, T., "Model-based fault detection with uncertainties in a reusable rocket engine," *2022 IEEE Aerospace Conference (AERO)*, IEEE, 2022, pp. 1–8. https://doi.org/https://doi.org/10.1109/aero53065.2022.9843212.

[9] Dalla Vedova, M. D. L., Germanà, A., Berri, P. C., and Maggiore, P., "Model-based fault detection and identification for prognostics of electromechanical actuators using genetic algorithms," *Aerospace*, Vol. 6, No. 9, 2019, p. 94. https://doi.org/https://doi.org/10.3390/aerospace6090094.

[10] Kawatsu, K., Tsutsumi, S., Hirabayashi, M., and Sato, D., "Model-based fault diagnostics in an electromechanical actuator of reusable liquid rocket engine," *AIAA Scitech 2020 Forum*, 2020, p. 1624. https://doi.org/https://doi.org/10.2514/6.2020-1624.

[11] Wheeler, P., "Technology for the more and all electric aircraft of the future," *2016 IEEE International Conference on Automatica (ICA-ACCA)*, IEEE, 2016, pp. 1–5. https://doi.org/https://doi.org/10.1109/ica-acca.2016.7778519.

[12] Garcia Garriga, A., Ponnusamy, S. S., and Mainini, L., "A multi-fidelity framework to support the design of More-Electric Actuation," *AIAA AVIATION 2018 Multidisciplinary Analysis and Optimization Conference*, 2018, p. 3741. https://doi.org/https://doi.org/10.2514/6.2018-3741.

[13] Garriga, A. G., Mainini, L., and Ponnusamy, S. S., "A machine learning enabled multi-fidelity platform for the integrated design of aircraft systems," *Journal of Mechanical Design*, Vol. 141, No. 12, 2019. https://doi.org/https://doi.org/10.1115/1.4044401.

[14] Mainini, L., "Structural assessment and sensor placement strategy for self-aware aerospace vehicles," *Structural Health Monitoring 2017*, 2017. https://doi.org/https://doi.org/10.12783/shm2017/14035.

[15] Mainini, L., and Willcox, K. E., "Sensor placement strategy to inform decisions," *18th AIAA/ISSMO Multidisciplinary Analysis and Optimization Conference*, 2017, p. 3820. https://doi.org/https://doi.org/10.2514/6.2017-3820.

[16] Berri, P. C., Dalla Vedova, M. D. L., and Mainini, L., "Real-time fault detection and prognostics for aircraft actuation systems," *AIAA Scitech 2019 Forum*, 2019, p. 2210. https://doi.org/https://doi.org/10.2514/6.2019-2210.

[17] Schmid, P. J., "Dynamic mode decomposition of numerical and experimental data," *Journal of fluid mechanics*, Vol. 656, 2010, pp. 5–28. https://doi.org/https://doi.org/10.1017/s0022112010001217.

[18] Schmid, P. J., Li, L., Juniper, M. P., and Pust, O., "Applications of the dynamic mode decomposition," *Theoretical and Computational Fluid Dynamics*, Vol. 25, No. 1, 2011, pp. 249–259. https://doi.org/https://doi.org/10.1007/s00162-010-0203-9.

[19] Wall, M. E., Rechtsteiner, A., and Rocha, L. M., "Singular value decomposition and principal component analysis," *A practical approach to microarray data analysis*, Springer, 2003, pp. 91–109. https://doi.org/https://doi.org/10.1007/0-306-47815-3_5.

[20] Kohonen, T., "The self-organizing map," *Proceedings of the IEEE*, Vol. 78, No. 9, 1990, pp. 1464–1480. https://doi.org/10.1109/5.58325.

[21] Kohonen, T., *Self-organizing maps*, Vol. 30, Springer Science & Business Media, 2012. https://doi.org/https://doi.org/10.1007/978-3-642-56927-2.

[22] Oja, E., "Simplified neuron model as a principal component analyzer," *Journal of mathematical biology*, Vol. 15, No. 3, 1982, pp. 267–273. https://doi.org/https://doi.org/10.1007/bf00275687.

[23] Peherstorfer, B., Willcox, K., and Gunzburger, M., "Survey of multifidelity methods in uncertainty propagation, inference, and optimization," *Siam Review*, Vol. 60, No. 3, 2018, pp. 550–591. https://doi.org/https://doi.org/10.1137/16m1082469.

[24] Song, J., Chen, Y., and Yue, Y., "A general framework for multi-fidelity bayesian optimization with gaussian processes," *The 22nd International Conference on Artificial Intelligence and Statistics*, PMLR, 2019, pp. 3158–3167.

[25] Grassi, F., Manganini, G., Garraffa, M., and Mainini, L., "Resource aware multifidelity active learning for efficient optimization," *AIAA Scitech 2021 Forum*, 2021, p. 0894. https://doi.org/https://doi.org/10.2514/6.2021-0894.

[26] Beran, P. S., Bryson, D., Thelen, A. S., Diez, M., and Serani, A., "Comparison of multi-fidelity approaches for military vehicle design," *AIAA AVIATION 2020 FORUM*, 2020, p. 3158. https://doi.org/ttps://doi.org/10.2514/6.2020-3158.vid.

[27] Močkus, J., "On Bayesian methods for seeking the extremum," *Optimization Techniques IFIP Technical Conference: Novosibirsk, July 1–7, 1974*, Springer, 1975, pp. 400–404. https://doi.org/https://doi.org/10.1007/978-3-662-38527-2_55.

[28] Snoek, J., Larochelle, H., and Adams, R. P., "Practical bayesian optimization of machine learning algorithms," *Advances in neural information processing systems*, Vol. 25, 2012.

[29] Frazier, P. I., "Bayesian optimization," *Recent advances in optimization and modeling of contemporary problems*, Informs, 2018, pp. 255–278. https://doi.org/https://doi.org/10.1287/educ.2018.0188.

[30] Reisenthel, P. H., and Allen, T. T., "Application of multifidelity expected improvement algorithms to aeroelastic design optimization," *10th AIAA multidisciplinary design optimization conference*, 2014, p. 1490. https://doi.org/https://doi.org/10.2514/6.2014-1490.

[31] Ghoreishi, S. F., and Allaire, D., "Multi-information source constrained Bayesian optimization," *Structural and Multidisciplinary Optimization*, Vol. 59, 2019, pp. 977–991. https://doi.org/https://doi.org/10.1007/s00158-018-2115-z.

[32] Charayron, R., Lefebvre, T., Bartoli, N., and Morlier, J., "Multi-fidelity Bayesian optimization strategy applied to Overall Drone Design," *AIAA SCITECH 2023 Forum*, 2023, p. 2366. https://doi.org/https://doi.org/10.2514/6.2023-2366.

[33] Williams, C. K., and Rasmussen, C. E., *Gaussian processes for machine learning*, Vol. 2, MIT press Cambridge, MA, 2006. https://doi.org/https://doi.org/10.7551/mitpress/3206.003.0004.

[34] Schulz, E., Speekenbrink, M., and Krause, A., "A tutorial on Gaussian process regression: Modelling, exploring, and exploiting functions," *Journal of Mathematical Psychology*, Vol. 85, 2018, pp. 1–16. https://doi.org/https://doi.org/10.1101/095190.

[35] Kennedy, M. C., and O'Hagan, A., "Predicting the output from a complex computer code when fast approximations are available," *Biometrika*, Vol. 87, No. 1, 2000, pp. 1–13. https://doi.org/https://doi.org/10.1093/biomet/87.1.1.

[36] Berkenkamp, F., Krause, A., and Schoellig, A. P., "Bayesian optimization with safety constraints: safe and automatic parameter tuning in robotics," *Machine Learning*, 2021, pp. 1–35. https://doi.org/https://doi.org/10.1007/s10994-021-06019-1.

[37] Huang, D., Allen, T. T., Notz, W. I., and Miller, R. A., "Sequential kriging optimization using multiple-fidelity evaluations," *Structural and Multidisciplinary Optimization*, Vol. 32, No. 5, 2006, pp. 369–382. https://doi.org/https://doi.org/10.1007/s00158-005-0587-0.

[38] Zhang, Y., Hoang, T. N., Low, B. K. H., and Kankanhalli, M., "Information-based multi-fidelity Bayesian optimization," *NIPS Workshop on Bayesian Optimization*, 2017, pp. 1–5.

[39] Takeno, S., Fukuoka, H., Tsukada, Y., Koyama, T., Shiga, M., Takeuchi, I., and Karasuyama, M., "Multi-fidelity Bayesian optimization with max-value entropy search and its parallelization," *International Conference on Machine Learning*, PMLR, 2020, pp. 9334–9345.

[40] Ruan, X., Jiang, P., Zhou, Q., Hu, J., and Shu, L., "Variable-fidelity probability of improvement method for efficient global optimization of expensive black-box problems," *Structural and Multidisciplinary Optimization*, Vol. 62, No. 6, 2020, pp. 3021–3052. https://doi.org/https://doi.org/10.1007/s00158-020-02646-9.

[41] Di Fiore, F., and Mainini, L., "Non-Myopic Multifidelity Bayesian Optimization," *arXiv preprint arXiv:2207.06325*, 2022.

[42] Kontogiannis, S. G., Demange, J., Savill, A. M., and Kipouros, T., "A comparison study of two multifidelity methods for aerodynamic optimization," *Aerospace Science and Technology*, Vol. 97, 2020, p. 105592. https://doi.org/https://doi.org/10.2514/6.2018-0415.

[43] Jones, D. R., Schonlau, M., and Welch, W. J., "Efficient global optimization of expensive black-box functions," *Journal of Global optimization*, Vol. 13, No. 4, 1998, p. 455. https://doi.org/https://doi.org/10.1023/A:1008306431147.

[44] Wilson, J. T., Hutter, F., and Deisenroth, M. P., "Maximizing acquisition functions for Bayesian optimization," *arXiv preprint arXiv:1805.10196*, 2018.

[45] Balaban, E., Bansal, P., Stoelting, P., Saxena, A., Goebel, K. F., and Curran, S., "A diagnostic approach for electro-mechanical actuators in aerospace systems," *2009 IEEE Aerospace conference*, IEEE, 2009, pp. 1–13. https://doi.org/https://doi.org/10.1109/aero.2009.4839661.

[46] Berri, P. C., Dalla Vedova, M., and Maggiore, P., "A Lumped Parameter High Fidelity EMA Model for Model-Based Prognostics," *Proceedings of the 29th ESREL, Hannover, Germany*, 2019, pp. 22–26. https://doi.org/https://doi.org/10.3850/978-981-11-2724-3_0480-cd.

[47] Berri, P. C., Dalla Vedova, M. D., Maggiore, P., and Viglione, F., "A simplified monitoring model for PMSM servoactuator prognostics," *MATEC Web of Conferences*, Vol. 304, EDP Sciences, 2019, p. 04013. https://doi.org/https://doi.org/10.1051/matecconf/201930404013.

[48] Berri, P. C., Dalla Vedova, M. D. L., and Mainini, L., "Learning for predictions: Real-time reliability assessment of aerospace systems," *AIAA Journal*, Vol. 60, No. 2, 2022, pp. 566–577. https://doi.org/https://doi.org/10.2514/1.j060664.

[49] Stevens, B. L., Lewis, F. L., and Johnson, E. N., *Aircraft control and simulation: dynamics, controls design, and autonomous systems*, John Wiley & Sons, 2015.

[50] Berri, P. C., Dalla Vedova, M. D. L., and Maggiore, P., "A smart electromechanical actuator monitor for new model-based prognostic algorithms," *International Journal of Mechanics and Control*, Vol. 17, No. 2, 2016, pp. 19–25. https://doi.org/https://doi.org/10.20944/preprints202301.0534.v1.

[51] Baldo, L., Bertone, M., Dalla Vedova, M. D. L., and Maggiore, P., "High-Fidelity Digital-Twin Validation and Creation of an Experimental Database for Electromechanical Actuators Inclusive of Failures," *2022 6th International Conference on System Reliability and Safety*, 2022, pp. 19–25. https://doi.org/https://doi.org/10.1109/ICSRS56243.2022.10067403.

[52] Di Fiore, F., Berri, P. C. C., and Mainini, L., "Rapid Assessment of Incipient Multimodal Faults of Complex Aerospace Systems," *AIAA SCITECH 2023 Forum*, 2023, p. 1092. https://doi.org/https://doi.org/10.2514/6.2023-1092.